Journal of Ceramic Processing Research. Vol. 12, No. 3, pp. 304~309 (2011)

J O U R N A L O F
Ceramic Processing Research

Consolidation of ultra fine WC-Co hard materials by a spark plasma sintering method and their mechanical properties

Hyun-Kuk Park[a], Hee-Jun Youn[a], Seung-Min Lee[a], Hee-Seon Bang[b] and Ik-Hyun Oh[a,*]

[a]*Korea Institute of Industrial Technology (KITECH), 1110-9 Oryong-dong, Buk-gu, Gwang-ju, Korea*

[b]*Department of Naval Architecture and Ocean Engineering, Chosun University, 375, Seosuk-dong, Dong-gu, Gwangju, 501-759, Korea*

Using the spark plasma sintering method, WC-6 wt.%Co hard materials were densified using an ultra fine WC-Co powder. The WC-Co was almost completely dense with a relative density of up to 100% after the simultaneous application of a pressure of 60 MPa and an electric current for 12 minutes without any significant change in the grain size. The average grain size of WC that was produced through SPS was about 270 nm. The hardness and fracture toughness of the dense WC-Co composites were also investigated.

Key words: Spark plasma sintering, WC-Co, Hard material, Sintering, Rapid sintering, Mechanical properties.

Introduction

Tungsten carbide-cobalt hard materials (WC-Co) are widely used for a variety of application such as machining, cutting and drilling. Morphologically, they consist of a high volume fraction of the "hard" hexagonal WC phase that is embedded within a soft and tough Co binder phase [1]. These WC-Co hard materials can be densified through liquid phase sintering, and the mechanical properties of these materials depend on their composition and microstructure (especially on the grain size of the carbide phase [2]). Thus, the grain growth of the carbide phase must be controlled during liquid phase sintering. In general, the mechanical properties, such as the hardness, wear resistance, and transverse rupture strength of the composites, increase with a decrease in the WC particle size [3]. Increasing the volume fraction of Co increases the fracture toughness at the expense of the hardness and the wear resistance [4, 5]. WC-cobalt and other similar cemented carbides are used for cutting tools because they possess a combination of a desirable hardness and a high fracture toughness from the respective contributions of the carbide and metallic phases. WC-Co can be densified through conventional sintering [6, 7], sintering in a spark plasma sintering (SPS) apparatus or a plasma pressure compaction apparatus [8, 9], and sintering from dynamic shock compression [10]. The primary concern in all these methods is the grain size of the WC component because the mechanical properties can be significantly improved by a finer grain size [11, 12]. Nanocrystalline materials have received much attention as advanced engineering materials because of their improved physical and mechanical properties [11, 12]. Undoubtedly, nanomaterials have attracted more attention because they possess a high strength, a high hardness and an excellent ductility and toughness [13, 14]. In recent days, nanocrystalline WC-Co cemented carbides have been developed using thermochemical and thermomechanical processes such as the spray conversion process (SCP) [15]. One advantage of SCP is that the WC particle size can be reduced below 100 nm. However, the WC grain size in the sintered WC-Co cemented carbides is much larger than the pre-sintered powders because of the rapid diffusion through the liquid phase during the conventional liquid phase sintering process. Therefore, although the initial WC size is less than 100 nm, the grain size rapidly increases up to 500 nm or larger during conventional liquid phase sintering [16]. Even when grain growth inhibitors are added to WC-Co, the WC grain size can increase up to 300 nm during the liquid phase sintering process [2, 17, 18]. Recent studies have shown that the high-frequency induction heated sintering (HFIHS) technique can be effective for sintering nanostructured materials in very short times (within 1 minute) [19-21]. So, controlling the grain growth during sintering is a key to the commercial success of nanostructured WC-Co composites. In this study, WC-Co was sintered using a rapid sintering process that is known as spark plasma sintering. This method combines a pulsed current with the application of a high pressure. The goal of this study was to produce dense, ultra-fine WC-6 wt.%Co hard materials in very short sintering times (< 12 minutes). Additionally, the mechanical properties of the WC hard materials were investigated.

*Corresponding author:
Tel : +82-62-600-6180
Fax: +82-62-600-6149
E-mail: ihoh@kitech.re.kr

Experimental Procedure

In this study, 99.95% pure tungsten carbide (0.4-0.5 μm, TaeguTec Ltd.) and 99.8% pure cobalt (1.6 μm, Alfa

Products) powders were used as the starting materials. Fig. 1 shows the FE-SEM images of the raw materials that were used. A particle size analyzer was used to examine raw WC and Co materials (Malvern, mastersizer 2000E). The WC and Co particle sizes were 0.2-0.3 μm and 10-20 μm, respectively. Additionally, the average grain sizes of WC and Co were about 0.3 μm and 15 μm with distributions of d(0.1) : 0.129 μm, d(0.5) : 0.199 μm, d(0.9) : 0.384 μm and d(0.1) : 6.413 μm, d(0.5) : 12.098 μm, d(0.9) : 23.844 μm, respectively. The mixed WC and Co powder with a molar ratio of 94 : 6 was milled in a high energy ball mill (planetary mill) at 250 rpm for 10 h. Tungsten carbide balls (6 mm in diameter) were used in a sealed cylindrical stainless steel vial with alcohol. The weight ratio of the balls-to-powder was 10 : 1, and the alcohol-to powder-was 2 : 1. The milling significantly reduced the grain size of the powder. The grain size and the internal strain were calculated using Stokes and Wilson's formula [22]:

$$b = b_d + b_e = k\lambda/(d\cos\theta) + 4\varepsilon\tan\theta \quad (1)$$

where, b is the full width at half-maximum (FWHM) of the diffraction peak after the instrumental correction; b_d and b_e are the FWHM for a small grain size and internal strain, respectively; k is a constant (with a value of 0.9); λ is the wavelength of the X-ray radiation; d and ε are the grain size and the internal strain, respectively; and θ is the Bragg angle. The parameters b and b_s follow Cauchy's form with the relationship: $B_0 = b + b_s$, where B_0 and b_s are the FWHM of the broadened Bragg peaks and a standard sample's Bragg peaks, respectively. Fig. 2 shows the XRD patterns of the raw powders and the milled WC-6 wt.% Co powder mixture. The FWHM of the milled powder was greater than the raw powders because of the reductions in the internal strain and the grain size. The average grain sizes of the milled WC and Co powders were 278 and 33 nm, respectively. Additionally, the milled powder ex-

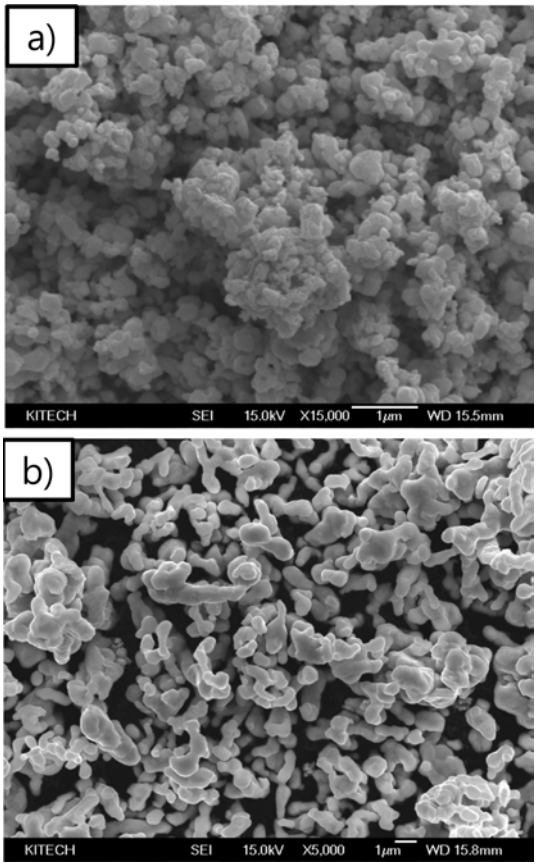

Fig. 1. FE-SEM images of the raw materials: a) WC and b) Co.

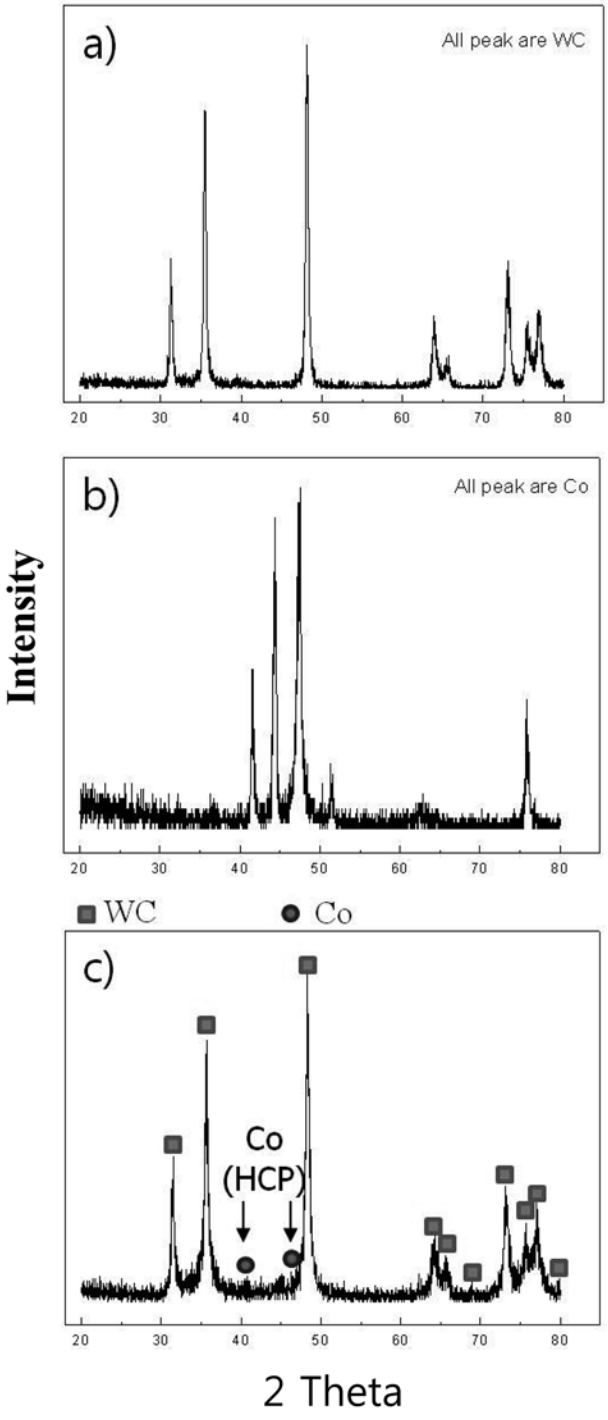

Fig. 2. XRD patterns of the WC-6 wt.% Co hard materials: a) WC, b) Co and c) ball milled.

hibited a particle size of about 100 nm and appeared to have a distribution of d(0.1) : 0.062 μm, d(0.5) : 0.094 μm, d(0.9) : 0.141 μm. After milling, the mixed powders were placed in a graphite die (outside diameter, 30 mm; inside diameter, 10 mm; height, 40 mm), and then placed into a spark plasma sintering system that was made by Sumitomo Coal Mining in Japan. A schematic diagram of this method is shown in Fig. 3. The SPS apparatus included a 25 V, 1000 A DC power supply (which provided a pulsed current for 12 ms with an off time of 2 ms through the sample and die) and a 10 ton uniaxial press. First, the system was evacuated, and a uniaxial pressure of 60 MPa was applied. Then a DC current was activated and maintained until the densification rate was negligible, as indicated by the observed shrinkage of the sample. The sample shrinkage was measured in real time using a linear gauge for the vertical displacement. The temperature was measured using a pyrometer that was focused on the surface of the graphite die. Depending on the heating rate, the electrical and thermal conductivities of the compact, and its relative density, the temperature on the surface and in the center of the sample could differ. The heating rate was approximately 100 K·minute^{-1} during this process. At the end of the process, the current was turned off, and the sample was allowed to cool to room temperature. The entire densification process using the SPS technique consisted of four major control stages, including the chamber evacuation, pressure application, power application, and cool down. The four major sintering stages are schematically shown in Fig. 4. This process was carried out under a vacuum of 6 Pa. The relative densities of the sintered samples were measured using the Archimedes method. Microstructural information was obtained from the product samples, which were polished and etched using a Murakami's reagent (5 g $Fe_3(CN)_6$, 5 g NaOH, and 50 ml distilled water), for 1 min at room temperature. The compositional and microstructural analyses of the products were carried out through X-ray diffraction (XRD) and field-emission scanning electron microscopy (FE-SEM).

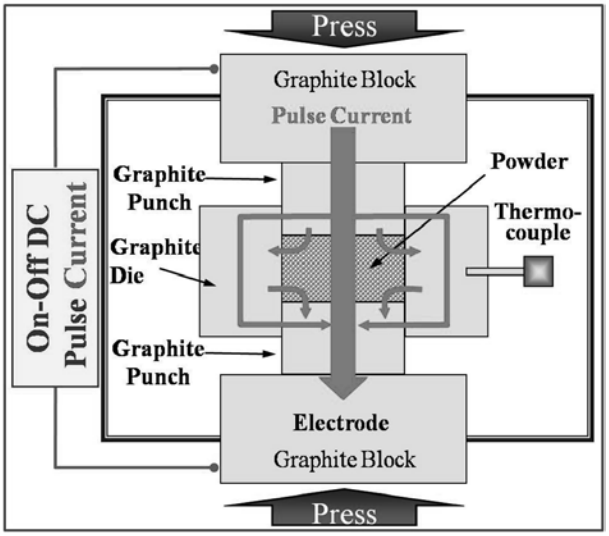

Fig. 3. Schematic diagram of the spark plasma sintering apparatus.

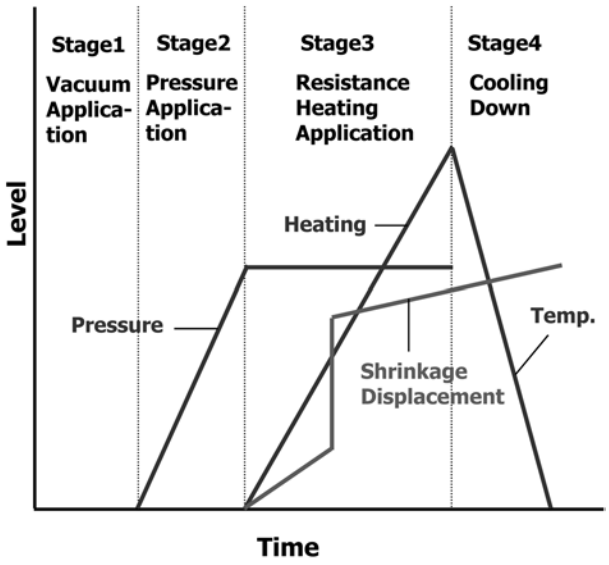

Fig. 4. Schematic representation of the temperature, pressure and shrinkage displacement profile during SPS.

The Vickers hardness was measured by performing indentation tests at a load of 30 kg and a dwell time of 15 s. The carbide grain size, d_{wc}, was obtained using the linear intercept method [23, 24].

Results

The XRD and FE-SEM analyses confirmed that a reaction did not take place and the shrinkage was not significant when a pulsed current was applied to the specimen with a small (thermal) expansion, abruptly increasing at approximately 650 °C. Fig. 5(a), (b) and (c) show the FE-SEM (field emission scanning electron microscopy) images of the powder after milling, the sample that was heated to 600 °C and the sample that was heated to 1200 °C, respectively. Fig. 6(a) and (b) show the presence of the reactants as separate phases. In Fig. 6(a), the X-ray diffraction results only exhibited peaks that pertained to the reactants, WC and the HCP crystal structure of Co. However, when the temperature was raised to 1200 °C, the starting powder completely reacted to produce fully dense products. These conclusions were supported by the X-ray diffraction analyses with peaks corresponding to the product phase, including WC and the FCC crystal structure of the Co phase, in Fig. 6(b). The solubility limit of tungsten in cobalt is about 10 at.% for the eutectic temperature of 1350 °C and strongly varies with the carbon content. Both tungsten and carbon stabilized the high temperature FCC phase of Co by impeding the martensitic transformation [23]. Therefore, the FCC phase of Co existed at room temperature. For pure WC, only peaks belonging to WC were observed, indicating that no compositional changes took place during sintering. No peaks for the sub-carbide W_2C or any impurity phase were present in Fig. 6(b). For the WC-6 wt.% Co cermets, only the WC and Co peaks were observed. In the XRD

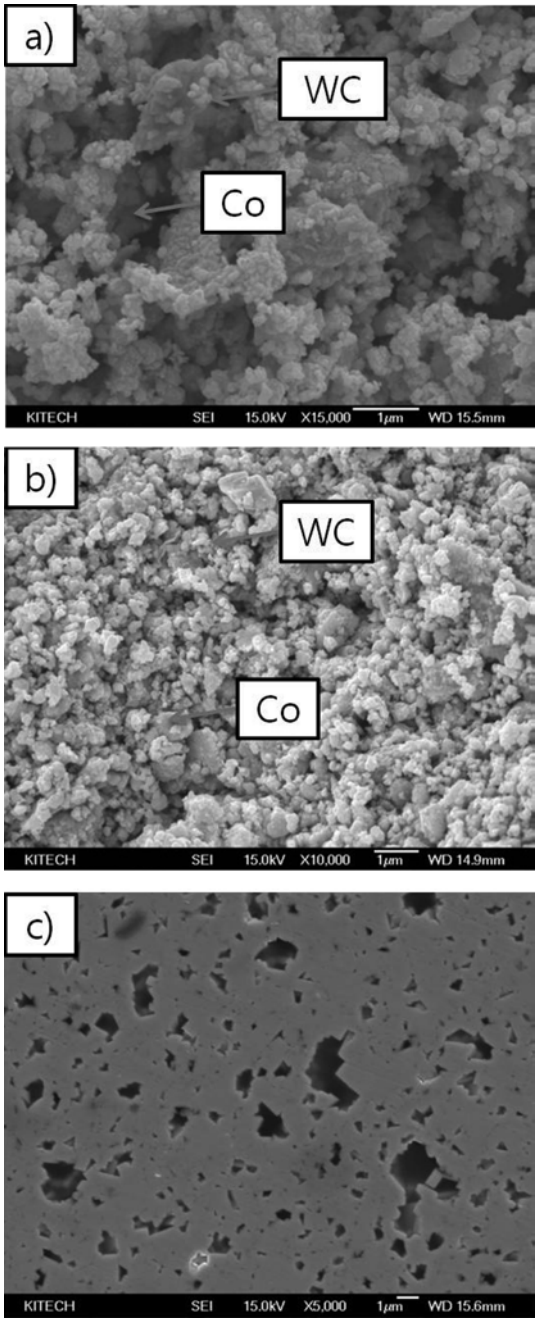

Fig. 5. FE-SEM images of the WC-6 wt.% Co system : a) after milling, b) before synthesis and c) after sintering.

patterns of the products, the solid solution was not observed because the solid solution peaks overlapped with Co.

Three different methods were used to calculate the grain size (Stokes and Wilson's formula, the Scherrer formula and the linear intercept method). The first expression, which was proposed by Stokes and Wilson's formula, produced an average grain size of about 309 nm for the sintered-body WC [21].

The second expression, which was proposed by the Scherrer Equation, suggested that the peak broadening of the WC-Co nanocrystallite was caused by its small crystal size [25]:

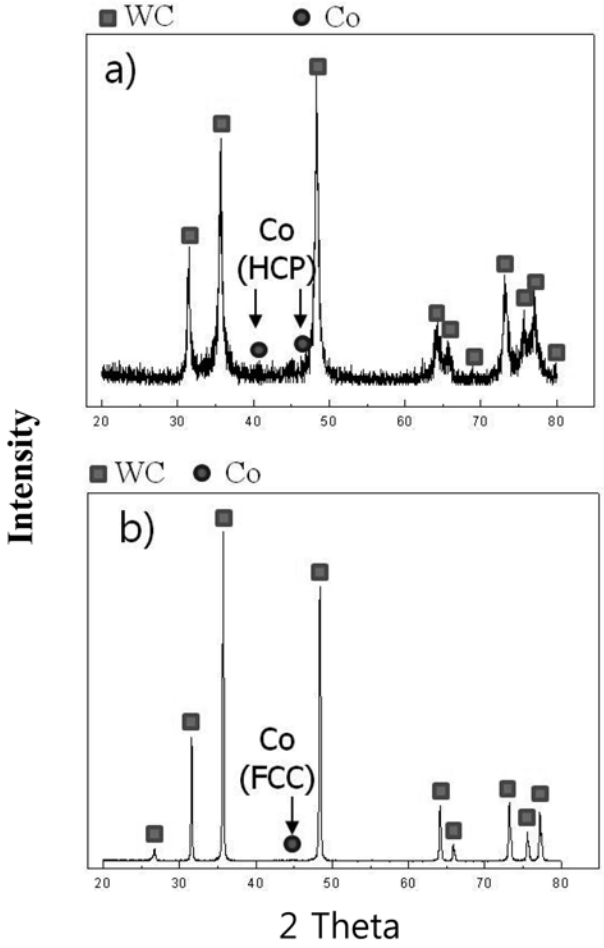

Fig. 6. XRD patterns of the WC-6 wt.% Co hard materials: a) ball milled and b) after sintering.

$$d = k\lambda / B_p \cos\theta \quad (2)$$

where, d is the crystal size; *k* is a constant (with a value of 0.9); λ is the wavelength, B_p is the broadening that was caused by the crystal size, and θ is the diffraction angle. The average crystal size of the sintered-body WC was 271 nm.

In the third expression, which was proposed by the linear intercept method, the sample surface preparation for the FE-SEM investigations was performed in accordance with the ASTM Method B657 for metallographic determination of microstructure in cemented carbides. Accordingly, the surface was polished in three steps. First, the samples were hand-ground on a 120 pm grade diamond grinder in order to remove at least 100 pm of the material. Then a 6 pm grade grinder was used. Finally, the samples were polished using a 1 μm grade diamond paste. The surface was etched using Murakami's reagent for 1 minute at room temperature, then rinsed with alcohol and dried with acetone through ultra sonication in order to identify the WC phase. Fig. 7 shows the FE-SEM images of the etched surfaces of the sample that was heated to 1200 °C at a pressure of 60 MPa. The structural parameters, i.e. the carbide grain size d_{wc} and the mean free path of the binder phase k (the average thickness of the binder phase), were obtained from the

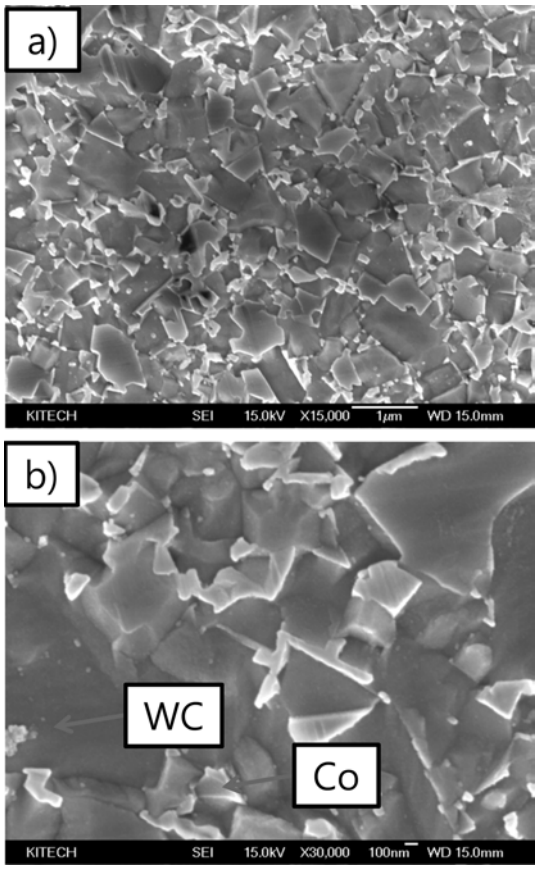

Fig. 7. FE-SEM image of the WC-Co hard materials: a) 1000 magnification and b) high magnification.

boundary intercepts with test lines on planar sections. The average number of intercepts per unit length of the test line was determined using the traces of the carbide/cobalt interface, $N_{WC/Co}$, and the carbide/carbide grain boundaries, $N_{WC/WC}$. From these quantities, the average carbide grain size and the mean free path were calculated using the following relationships [22, 23]:

$$d_{WC} = 2V_{WC}/(2N_{WC/WC} + N_{WC/Co}) \quad (3)$$

where, V_{WC} is the carbide volume fraction, and V_{Co} is the binder volume fraction. The average size of about 300 nm for these grains in the nearly fully dense WC-6 wt.% Co composites was determined using the linear intercept method. These three different methods produced similar average grain sizes of 271, 300 and 309 nm, respectively. Thus, a fine structure was obtained without any grain growth during sintering using the SPS method.

The Vickers hardness measurements were taken on the polished sections of the binder WC-6 wt.% Co hard materials using a 30 kgf load at a dwell time of 15 s. At large enough loads, the indentations produced median cracks that emanated from the corners of the indent. The fracture toughness was calculated from the cracks that were produced from the indentations under large loads. The length of these cracks was used to estimate the fracture toughness of the material through the Anstis expression [26]:

$$K_{IC} = 0.016(E/H)^{1/2}P/C^{3/2} \quad (4)$$

where, E is the Young's modulus, H is the indentation hardness, P is the indentation load, and C is the trace length of the crack that was measured from the center of the indentation. The modulus was estimated from the rule mixtures with a volume fraction of 0.103 of Co and 0.897 WC using E(Co) = 209 GPa and E(WC) = 696 GPa. The elastic module E of WC-6 wt.% Co was about 666.8 GPa. As with the hardness values, the toughness values were derived from the average of five measurements. The calculated hardness and fracture toughness values of WC-6 wt.% Co with a WC size of about 270 nm were 1755.81 kg/mm^2 and 25.62 MPa·m$^{1/2}$, respectively, after SPS at 60 MPa and 1200 °C. Table 1 shows the calculated structural characteristics of the WC-Co composites, including the hardness and fracture toughness values, from the above formulas, based on the planar section measurements.

A typical indentation pattern for the WC-6 wt.% Co composite is shown in Fig. 8(a). Typically, one to three additional cracks propagated from the indentation corner. A higher magnification view of the indentation median crack in the composite is shown in Fig. 8(b). This figure shows that the crack propagated along the phase boundary of WC and Co. The crack segments ran both along the WC-Co phase boundaries (white arrows) and through the WC phase itself (black arrows). The Co binder phase is known to prevent crack propagation in the cemented carbide by shielding a stress field in front of the crack tip or by bridging the crack forming ligaments behind the crack tip [20, 27, 28].

Table 1. Comparison of the mechanical properties of WC-Co that was sintered in this study along with previously reported values

Ref.	Binder contents (wt.%)	Relative density (%)	Grain Size (μm)	HV (kg/mm^2)	K_{IC} (MPa·m$^{1/2}$)
[25]	10 Co	-	0.35~0.43	1800	
[26]	10 Co	98.9	1.9	1333	13.5
[27]	10 Co	99.5	0.38	1756	11.6
[28]	95WC–3TiC–1.5TaC–0.5NbC	-	1.3	1900	8
[29]	94WC–6Mo2C	-	0.25	2400	8.4
[30]	WC–2.9Co	98.3	0.94	2014	6.5
This work	WC-6Co	100	0.3	1756	25.6

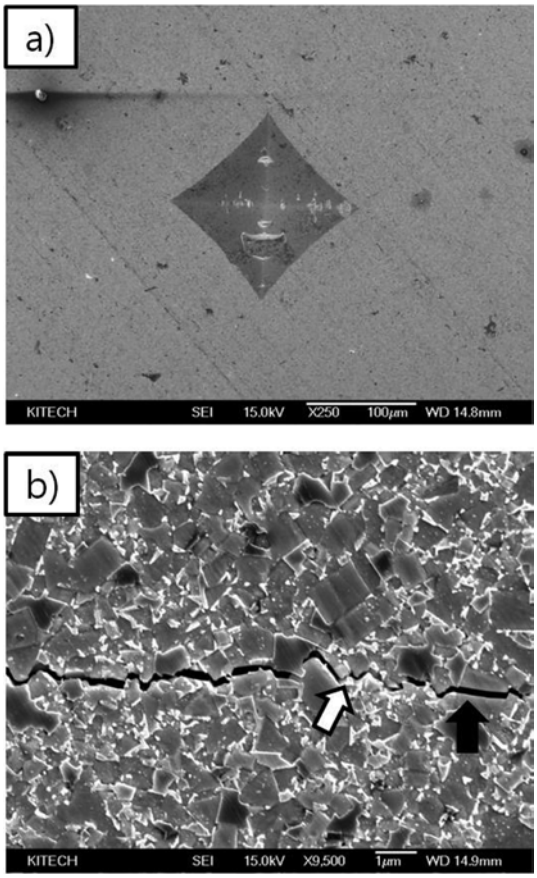

Fig. 8. (a) Vickers hardness indentation and (b) median crack propagation in the WC-6 wt.% Co composite.

Summary

The WC-6 wt.% Co hard materials were rapidly consolidated using the spark plasma sintering method with ultra fine WC and Co powders. Almost fully dense WC-6 wt.% Co was obtained within 12 minutes. The densification temperature of WC was reduced remarkably through the addition of Co. The grain size of WC was about 270 nm, and the nano-structure was obtained without any grain growth during sintering using the SPS method. The fracture toughness and the hardness values of WC-6 wt.% Co were 25.6 MPa·$m^{1/2}$ and 1755.8 kg/mm^2, at 60 MPa and 1200 °C.

References

1. K. Mohan and P.R. Strutt, Nanostruct Mater. 7(1996) 547-555.
2. B.K. Kim, G.H. Ha and D.W. Lee, J Mater Process Technol 63(1997) 317-321.
3. F.L. Zhang, C.Y. Wang and M. Zhu, Scripta Mater. 49 (2003) 1123-1128.
4. S.G. Shin, Met. Mater. 6(2000) 195-201.
5. M.J. Ledoux, C.H. Pham, J. Guille and H. Dunlop, J. Catal. 134 (1992) 383-398.
6. W. Acchar, U.U. Gomez, Kaysser WA, Goring J., Mater. Charact. 43 (1999) 27-32.
7. T. Ungar and A. Borbely, Nanostruct Mater. 11 (1999) 103-113.
8. A. Hirata, H. Zheng and M. Yoshikawa, Diam. Relat. Mater. 7 (1998) 1669-1674.
9. T.S. Srivatsan, R. Woods, M. Petraroli and T.S. Sudarshan, Powder Technol. 122 (2002) 54-60.
10. K. Yamada, J. Alloys & Compd. 305 (2000) 253-258.
11. M.S. El-Eskandarany, J Alloys & Compd. 305 (2000) 225-238.
12. L. Fu, L.H. Cao and Y.S. Fan, Scripta Mater. 44 (2001) 1061-1068.
13. K. Niihara and A. Nikahira, Trieste, Italy: Elsevier Scientific Publishing Co; 1990.
14. S. Berger, R. Porat and R. Rosen, Prog. Mater. 42 (1997) 311-320.
15. Z. Fang and J.W. Eason, Int. J. Ref. Met. Hard Mater. 13 (1995) 297-303.
16. M. Sommer, W.D. Schubert, E. Zobetz and P. Warbichler, Int. J. Ref. Met. Hard Mater. 20 (2002) 41-50.
17. S.I. Cha, S.H. Hong and B.K. Kim, Mater. Sci. Eng. 351 (2003) 31-38.
18. S.I. Cha, S.H. Hong, G.H. Ha and B.K. Kim, Scripta Mater. 44 (2001) 1535-1539.
19. H.C. Kim, I.J. Shon and Z.A. Munir, J. Mater. Sci. 40 (2005) 2849-2854.
20. H.C. Kim, D.Y. Oh and I.J. Shon, Int. J. Ref. Met. Hard Mater. 22 (2004) 197-203.
21. H.C. Kim, H.K. Park, I.K. Jung, I.Y. Ko and I.J. Shon, Cermics Int. 34 (2008) 1419-1423
22. F.L. Zhang, C.Y. Wang and M. Zhu, Scripta Mater. 49 (2003) 1123-1128.
23. K. Jia, T.E. Fischer and G. Gallois, Nanostruct Mater. 10 (1998) 875-891.
24. J.H. Han and D.Y. Kim, Acta Mater. 46 (1998) 2021-2028.
25. P. Scherrer and N.G.W. Gottingen, Math-Pys. Kl. 2 (1918) 96-100.
26. G.R. Anstis, P. Chantikul, B.R. Lawn and D.B. Marshall, J. Am. Ceram. Soc. 64 (1981) 533-538.
27. L.S. Sigl and H.F. Fischme ister, Acta Metall. 36 (1988) 887-897.
28. L.S. Sigl, P.A. Mataga, B.J. Dalgleish, R.M. McMeeking and A.G. Evans, Acta Metall. 36 (1988) 945-958.
29. H. Engqvist, G.A. Botton, N. Axen and S. Hogmark, J. Am. Ceram. Soc. 83 (2000) 2491-2497.
30. C.D. Park, H.C. Kim, I.J. Shon and Z.A. Munir, J. Am. Ceram. Soc. 85 (2002) 2670-2677.